Metallography, Microstructure, and Analysis (2021) 10:525–533
https://doi.org/10.1007/s13632-021-00762-6

TECHNICAL ARTICLE

Effects of Partitioning Time and Temperature on the Microstructure and Mechanical Properties of a High Strength Microalloyed Steel

Ali Almasi[1] · Abbas Kianvash[1] · Abolfazl Tutunchi[1]

Received: 11 May 2021 / Revised: 28 July 2021 / Accepted: 28 July 2021 / Published online: 17 August 2021

Abstract

In the present study, in a quenching–partitioning (Q–P) process, the effects of partitioning time (Pt) and partitioning temperature (PT) on the mechanical and microstructural properties of a microalloyed Fe-0.21C-1.5Si-2.2Mn-0.054Al-0.08Ti steel were studied. The XRD and SEM results confirmed increases in retained austenite (γ_R) volume fraction (V_{γ_R}) and γ_R carbon concentration by increasing Pt and PT. XRD patterns confirmed reduction in V_{γ_R} by further increasing the Pt and PT over 500 s and 390 °C, respectively, due to super-saturation of austenite (γ) with carbon. PT of 390 °C and Pt of 500 s were recorded as the optimum values for PTs and Pts, which allowed the present steel to obtain higher formability and higher fracture strain characteristics, while retaining higher hardness and strength. The highest yield and tensile strength, hardness and fracture elongation were obtained for the sample partitioned at 390 °C for about 500 s, which were about 741 MPa, 1366 MPa, 322 HB and 25.2%, respectively.

Keywords Quenching and partitioning (Q–P) · Retained austenite · Yield strength · Tensile strength · Hardness · Fracture elongation

Introduction

Quenching and partitioning process (Q–P) has been developed over the last decade in order to improve the ductility of parts under the premise of ensuring the high strength [1]. Quenched and partitioned steel exhibits an excellent combinations of strength and ductility with a final microstructure containing ferrite, martensite (M), and γ_R, which is suitable for body parts in a new generation of advanced automobiles [2]. In the Q–P process, austenitized steel is cooled down to a temperature named as quench temperature (QT), which is between M transformation starting (M_s) and finishing temperature (M_f). After partitioning in a temperature range between $M_s - M_f$, the sample is cooled in water down to the room temperature [3].

The main aim of the Q–P process is to improve the steels ductility and strength simultaneously, which is performed by stabilization of the γ_R below M_f. Suitable alloying elements such as Ti, Nb, and V play an important role in improving the strength of steels, mainly through precipitation hardening and grain refinement [4, 5]. On the other hand, partitioning process can increase the strength and ductility of steels by stabilization of austenite even at room temperature. During service cycles, transformation of strain-induced γ_R to M can improve the sample's mechanical properties. Therefore, it is very important to control and optimize V_{γ_R} in the steel during the partitioning process [6]. Austenite stability is affected by the partitioning temperature (PT), austenite grain size and carbon content in γ_R [7–11]. It has been confirmed that an increase in the austenite carbon content results in an increase in the austenite stability against strain-induced transformation [12–14]. Furthermore, the presence of some elements such as Ti, Mo and Nb in steel will cause simultaneous increase in strength and ductility [15, 16]. Combination of these elements with some carbon leads to the formation of carbides and thus improves the mechanical performance of steels [17, 18]. Carbides can prevent the possible bainitic transformation, which will lead to subsequent increase in V_{γ_R} [19]. In the partitioning process, carbon atoms diffuse from M to γ that lead to an increase in the austenite carbon content and therefore increase the austenite stability [20–22]. There are three main methods for Q–P process (Fig. 1). In method

✉ Abbas Kianvash
akianvash@tabrizu.ac.ir

[1] Department of Materials Engineering, Institute of Mechanical Engineering, University of Tabriz, 51666-16471 Tabriz, Iran

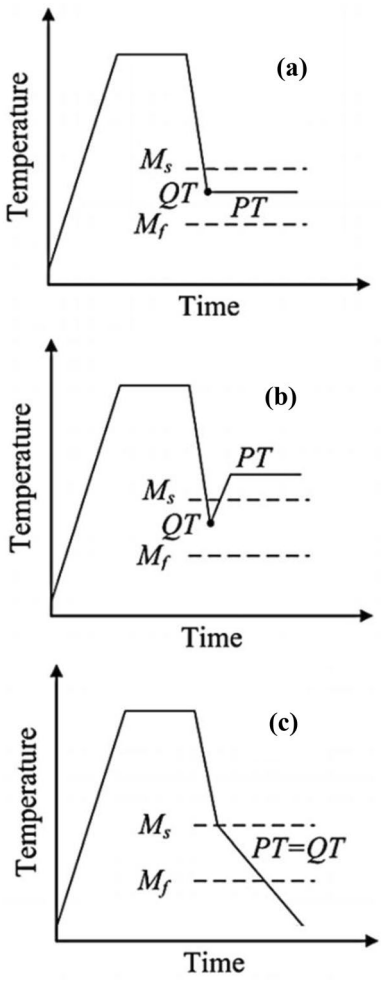

Fig. 1 Three methods used in Q–P proccesses [23]

1 (Fig. 1a), the PT is constant and equal to the quenching temperature (QT). Partitioning, in this case, will continue until the partial martensitic transformation is completed. In method 2 (Fig. 1b), PT is constant and almost greater than the QT. Method 2 that is called a 'II step process can be designed below or above M_s. In method 3 (Fig. 1c), partitioning and M transformation are performed simultaneously [23].

In all the three methods, carbon enriched γ_R can again transform to M at low temperatures. Figure 2 shows the chemical free energy of γ and M versus temperature. At T_0, the γ free energy is equal to that of M, which results in the coexistence of M and γ. Because of lower free energy, γ is more stable above T_0 and M is more stable below T_0. At temperatures below T_0, the transformation of M to γ suppresses because of positive Gibbs free energy change ($\Delta G°$). At temperatures between M_s and T_0 such as T_1, undercooling is not enough to start the transformation but the transformation may start if sufficient mechanical driving force is introduced [24–26]. At temperatures above T_0 such as T_2,

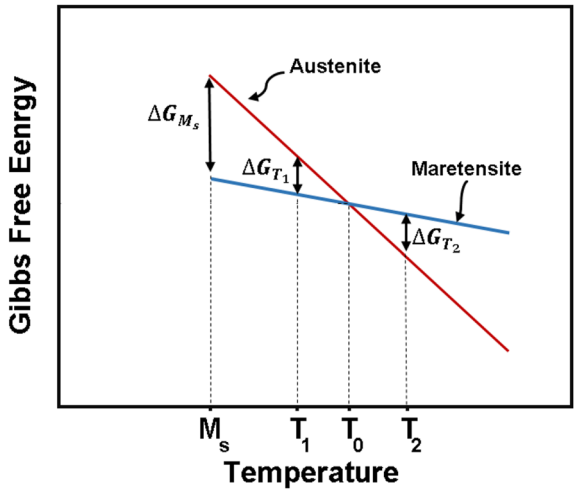

Fig. 2 γ and M Gibbs free energy versus temperature

M to γ transformation occurs spontaneously due to sufficient driving force. It is expected that an increase in the PT to $T > T_0$ leads to an increment in the V_{γ_R} due to the more decreasing of ΔG^o and therefore increase in the transformation driving force. However, by further increase of PT, γ could be supersaturated with carbon due to higher diffusion of carbon almost. This leads to reduction of carbon content in martensite and thus reduces the martensitic slabs strength [11, 27, 28]. Partitioning kinetics and therefore the sample microstructure and strength are strongly affected by Pt and PT. Therefore, the mechanical properties of the samples such as UTS and total elongation will be varied by Pt and PT. For most applications such as automobile bodies, the steel sheets must illustrate both higher UTS and higher fracture elongation [29]. Therefore, optimization of the partitioning parameters is very important in these types of steels, in order to attain higher UTS and ductility, simultaneously. The aim of the present research is to study the effects of Pt and PT on the microstructure, and mechanical properties of high strength microalloyed Fe-0.21C-1.5Si-2.2Mn-0.054Al-0.08Ti steel.

Experimental

The chemical composition of the steel used in the present experiment is represented in Table 1. The steel ingot was prepared by melting together the elemental components in a vacuum induction furnace. The cast ingot was then homogenized at ~ 1200 °C for about 180 min under an Ar atmosphere. It was hot rolled at ~ 1000 °C in three passes to a thickness of around 1.5 mm.

Time–temperature–transformation (TTT) diagram of the present steel was constructed using JMatPro software. The

Table 1 Chemical composition of the steel used in the present experiment

Fe, wt.%	C, wt.%	Si, wt.%	Mn, wt.%	Al, wt.%	Ti, wt.%
95.5	0.21	1.5	2.2	0.054	0.08

M_s of the steel determined by the JMatPro was compared with that of the one calculated by Rowland and Lyle equation (Eq 1) according to the steel chemical composition, in which X_i represents the elements concentrations in weight percentages [36].

$$M_s\ (^\circ\mathrm{C}) = 499 - 324\,X_C - 32.4\,X_{Mn} - 10.8\,X_{Si} \quad (1)$$

M_s determined by the software (352 °C) was quite comparable with that of the calculated one using Eq 1 (344 °C). The steel specimens in the form of tensile samples were first austenitized at ~ 880 °C for 5 min and were then quenched in molten bath at ~ 300 °C and kept in it for 4 s. To optimize the PT, six PTs of 290, 310, 330, 370, 390 and 410 °C were examined according to Fig. 3a. After quenching, each sample was immediately transferred to a partitioning molten bath at one of the above temperatures and partitioned for 90 s and was then cooled to ambient temperature by water quenching. The effects of PT on the microstructure, YS, UTS, and fracture elongation of specimens were then studied in an attempt to optimize the PT. To optimize the Pt, 5 specimens were partitioned at the optimized PT for 10, 100, 300, 500 and 1000 s and then water quenched to ambient temperature (Fig. 3b).

The phase analyses and microstructural studies of the samples were examined using x-ray diffraction (Siemens D5000, Cu Kα radiation ($\lambda = 1.54$ Å)) and scanning electron microscopy (SEM), respectively. The tensile properties and microhardness of the samples were measured using a universal stress–strain tester and a Brinell microhardness tester, respectively.

Results and Discussion

Thermo-Calc software was used to depict the steel's equilibrium phase diagram in order to define critical temperatures: Ae_1', Ae_1 and Ae_3. Ae_1' represents cementite totally dissolving temperature (Fig. 4). Ae_1 is the temperature at which austenite volume fraction is zero. At the temperatures below Ae_1, microstructure of the steel involves ferrite and cementite. At the temperatures above Ae_3, the sample will be completely austenitized. According to Fig. 4, the sample should be austenitized above 780 °C. Furthermore, it is necessary to calculate M_s in order to design the heat treating process.

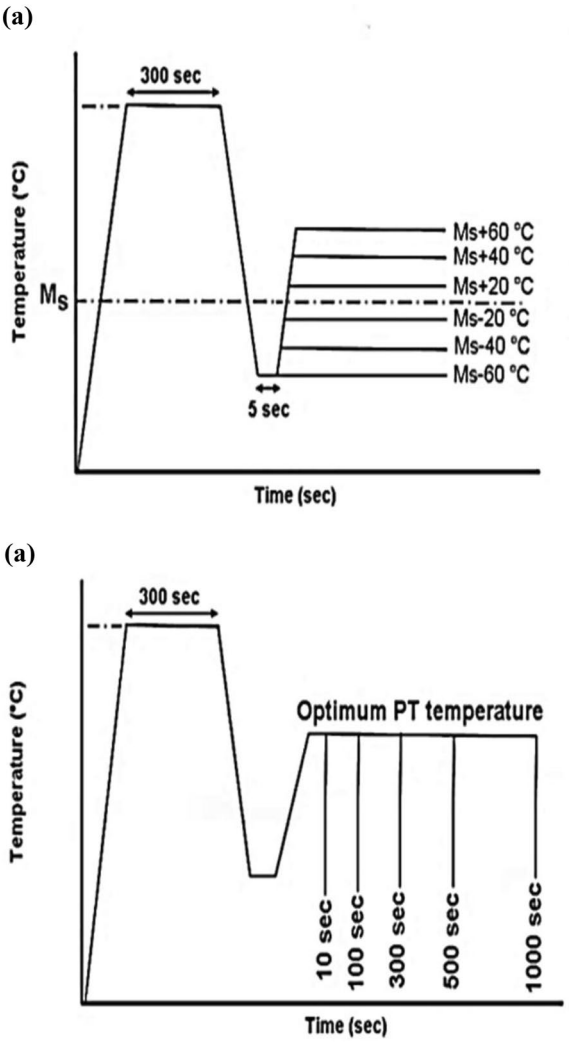

Fig. 3 Schematics of the Q–P process used in the present experiment partitioning at the various temperatures (**a**) and various times (**b**)

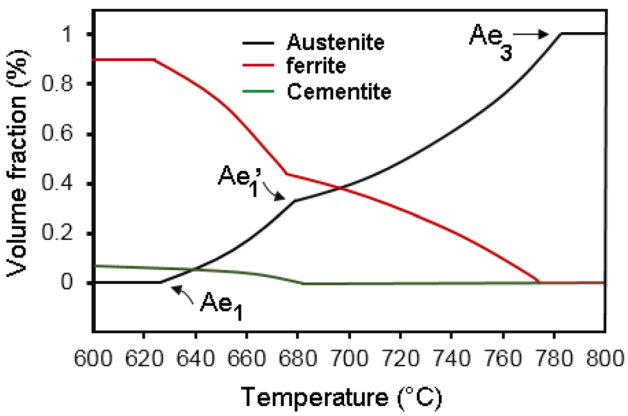

Fig. 4 Equilibrium V_α, V_γ and V_{Fe_3C} vs. temperature in the present steel determined using the Thermo-Calc

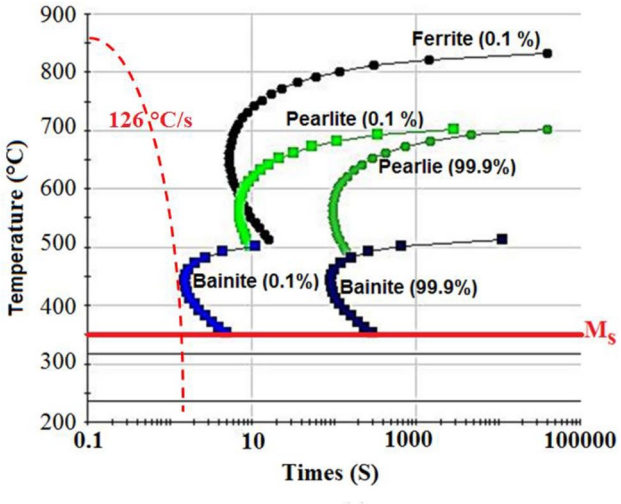

Fig. 5 TTT diagram of the present steel which is developed using the JMatPro package

The T–T–T diagram of the present steel, which is constructed using the JMatPro package, is shown in Fig. 5. From this diagram, M_s was determined as ~ 350 °C which is pretty close to one calculated using the Rowland and Lyle Eq. (344 °C). A cooling rate of ~ 126 °C/s was recorded as the critical cooling rate. By the JMatPro software, we realized that to suppress the formation of bainite, the austenitized samples (austenitized at 880 °C) must be cooled to QT by a cooling rate more than 126 °C/s. In the present experiment, a cooling rate of ~ 140 °C/s was selected as the first quenching step (cooling from austenitizing temperature to QT). This cooling rate was performed by keeping the austenitized samples at the quenching molten bath for about 4 s (the temperature of the samples was controlled by an infrared Thermometer throughout this steep). The partitioning temperatures (PTs) were selected as $M_s \pm 60$ °C, thus they were chosen between 290 and 410 °C, according to Fig. 3a.

SEM images of the samples quenched and partitioned in the temperature range of 290–410 °C are shown in Fig. 6. The microstructure of all the samples was consisted of α, M, and γ_R phases, however, it seems that by increasing the PT, the V_{γ_R} is increased. Normally, QP steels have no ferrite phase. The samples of this research, which were the low

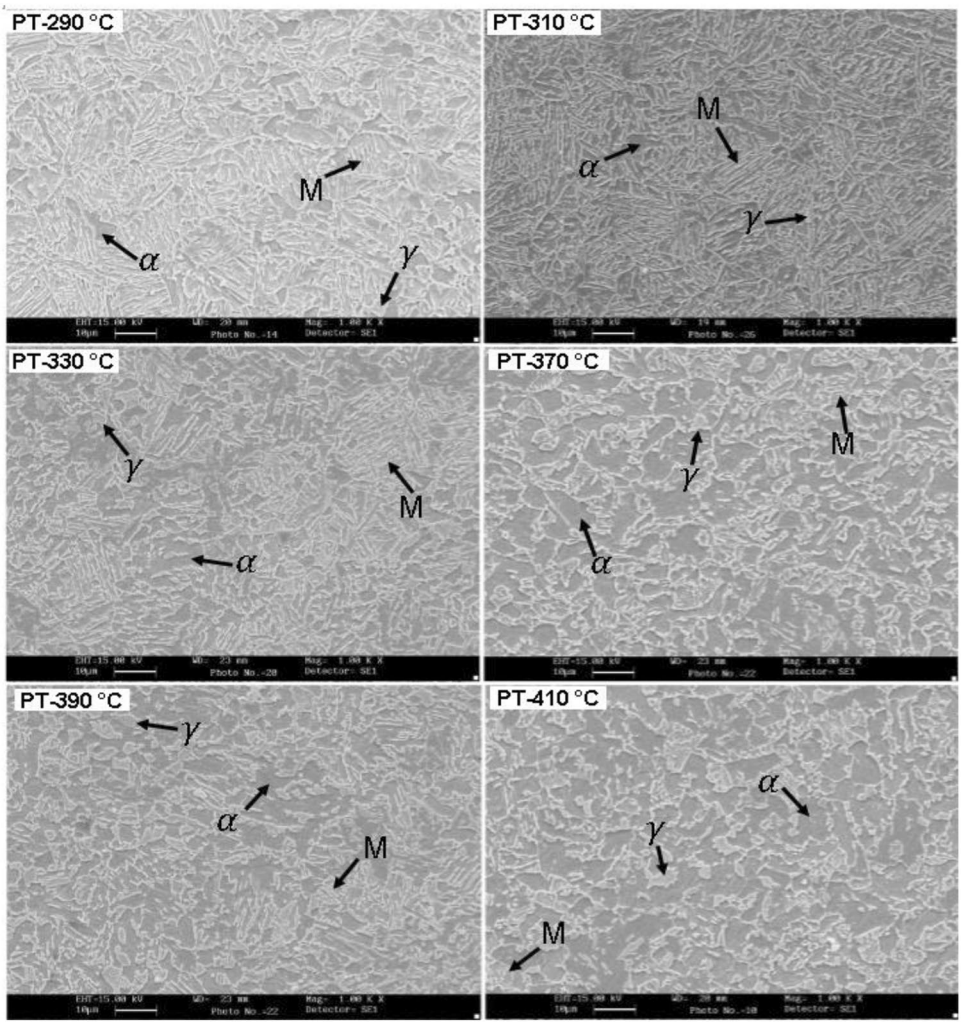

Fig. 6 SEM images of the samples partitioned at various temperatures

carbon steels, were austenized in the double phase region of $\alpha + \gamma$. Therefore, α phase was formed in the samples microstructure throughout austenitizing step (before quenching in bath furnace). Figure 7 represents the XRD patterns for the samples partitioned at the temperatures of 290–410 °C. The peaks assigned to γ_R were found to be very weak in comparison to those of α. The V_{γ_R} was calculated according to Eq 2, where I_γ is the average integrated intensities of (200), (220) and (311) peaks of austenite; Ia is the average integrated intensities of (200) and (211) peaks of M [16]. Carbon content in γ_R was calculated in weight percentage using Eq 3, in which a_γ is the lattice parameter of γ_R calculated by Eq 4, where λ, θ, and h, k, l are the XRD laser source wavelength, diffraction angle and Miller indices of (200) plane, respectively [37, 38].

$$V_\gamma = 1.4I_\gamma/(I_\alpha + 1.4I_\gamma) \tag{2}$$

$$C_\gamma = (a_\gamma - 3.547)/0.046 \tag{3}$$

$$a_{(hkl)} = \frac{\lambda}{2 \cdot \sin\theta} \cdot (h^2 + k^2 + l^2)^{1/2} \tag{4}$$

The structural characteristics of γ_R in the samples partitioned at 290–410 °C are shown in Table 2. The variations in V_{γ_R} and γ_R carbon content (C_{γ_R}) versus PT are shown in Fig. 8. There is an increasing tenderly in V_{γ_R} and C_{γ_R} by increasing the PT. The increase in V_{γ_R} by increasing PT could be due to increase in C_{γ_R} which the latter increases the γ_R stability. By increasing PT to 410 °C, γ_R has been

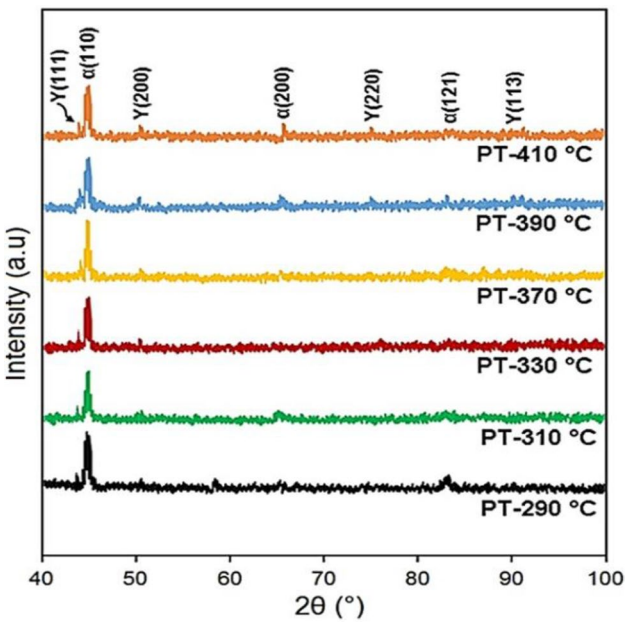

Fig. 7 XRD patterns of the samples partitioned at the temperature range of 290–410 °C

Table 2 Structural characteristics obtained for the samples partitioned at 290–410 °C, using XRD patterns.

Sample name	V_γ, %	$\theta_{(200)\gamma}$, °	a_γ, °A	C_γ, wt.%
PT-290 °C	7.68	25.631	3.559	0.28
PT-310 °C	8.77	25.615	3.563	0.35
PT-330 °C	9.84	25.604	3.562	0.37
PT-370 °C	13.61	25.521	3.574	0.60
PT-390 °C	28.1	25.390	3.591	0.96
PT-410 °C	22.51	25.412	3.589744	0.92

supersaturated by carbon, which has led to rejection of carbon from γ_R to its surrounding phase (α phase) and therefore increasing the volume fraction of α, simultaneously. Rejection of carbon from γ_R resulted in a decrement in C_{γ_R} and V_{γ_R}, finally. In fact, the carbon concentration of γ_R perhaps was more than that of α and martensite phases at PT = 410 °C, which has resulted in diffusion and rejection of carbon atoms from γ_R (region of higher concentration) to α and martensite phases (regions of lower concentration). Rejection and therefore decreasing of carbon content of γ_R lead to decrease of γ_R stability. By decreasing of γ_R stability, the transformation of $\gamma_R \rightarrow \alpha + M$ can be occurred throughout the partitioning and quenching process, which results in an increase of the volume fraction of α.

The study of steel behavior against sudden and rapid strain is also very important in the present experiment. The tensile stress–strain curves of the samples partitioned at the temperatures of 290–410 °C are shown in Fig. 9. The UTS, YS, and fracture strength of these samples are given in Table 3. By increasing the PT from 290 to 390 °C, UTS of the samples increases from 786 to 1052 MPa. Further increasing the PT from 390 to 410 °C resulted in a slight reduction in UTS value to 1035 MPa. This could be related

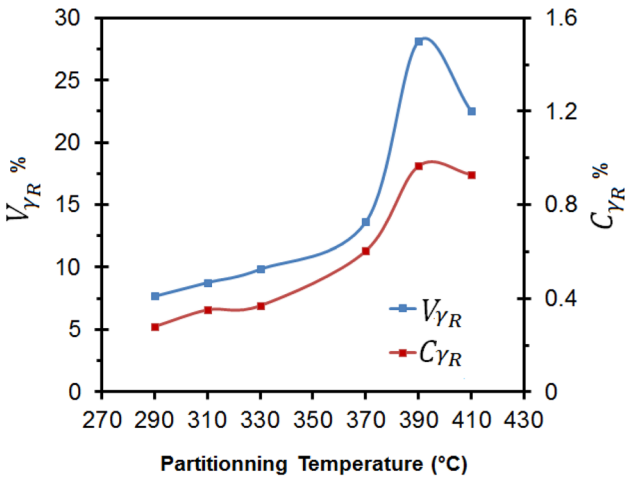

Fig. 8 Variations in V_{γ_R} and C_{γ_R} as a function of PT

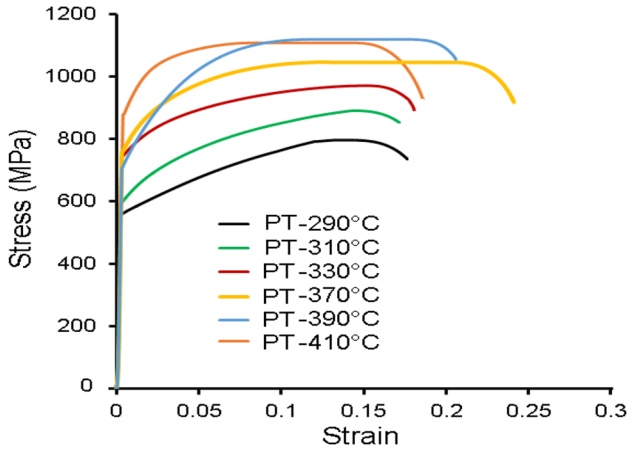

Fig. 9 The stress–strain curves for the samples partitioned at the temperature range of 290–410 °C

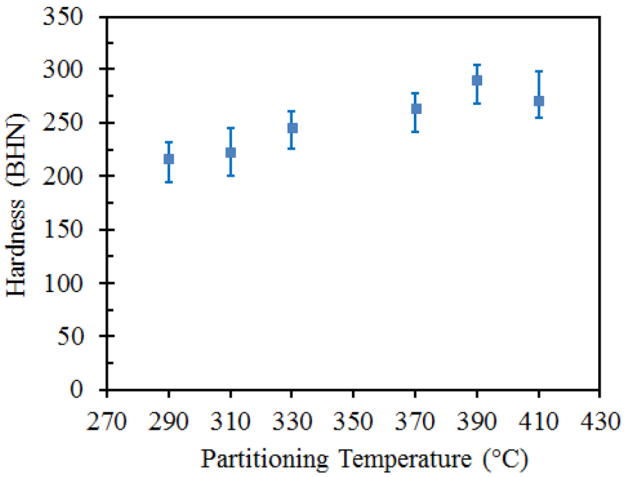

Fig. 10 Hardness of the samples partitioned at the temperature range of 290–410 °C

Table 3 UTS, YS and fracture strength of the samples partitioned at the temperature range of 290–410 °C

Sample designation	UTS, MPa	Y.S, MPa	Total elongation, %
PT-290 °C	786 ± 7	556 ± 9	17.59 ± 0.7
PT-310 °C	895 ± 7	611 ± 6	17.52 ± 0.4
PT-330 °C	953 ± 5	739 ± 8	18.16 ± 0.9
PT-370 °C	1016 ± 9	767 ± 9	24.76 ± 0.7
PT-390 °C	1052 ± 8	726 ± 5	18.25 ± 0.6
PT-410 °C	1039 ± 5	865 ± 7	21.33 ± 0.8

to a reduction in γ_R content in this sample in comparison to that of the sample partitioned at 390 °C. However, YS increased by increasing the PT up to 410 °C. The highest total elongation was obtained for the sample partitioned at 370 °C. As seen in Fig. 6, the volume fraction of α increased by increasing the PT to the temperatures above 370 °C, which has been led to an increase in the total elongation. BCC crystal structures (such as α) manifest low ductility compared to the FCC crystal structures (such as γ). The variation in microhardness of the samples partitioned at 290–410 °C is shown in Fig. 10. Maximum hardness was recorded for the sample partitioned at 390 °C (290 HB) due to the higher C_{γ_R} of γ_R (Figs. 11, 12).

According to the results obtained within the scope of the present study, the temperature interval of 370–410 °C was recognized as the suitable PT. Within this temperature interval, the PT of 390 °C was chosen as a typical suitable temperature to optimize the Pt. For this, Pts of 10, 100, 300, 500 and 1000 s at the PT of 390 °C were evaluated. SEM images of the samples partitioned at these Pts are shown in Fig. 11a–e. V_{γ_R} in the samples partitioned for 10 and 100 s was found to be relatively low. This could be related to insufficient time for carbon diffusion from M to γ_R. Thus, the

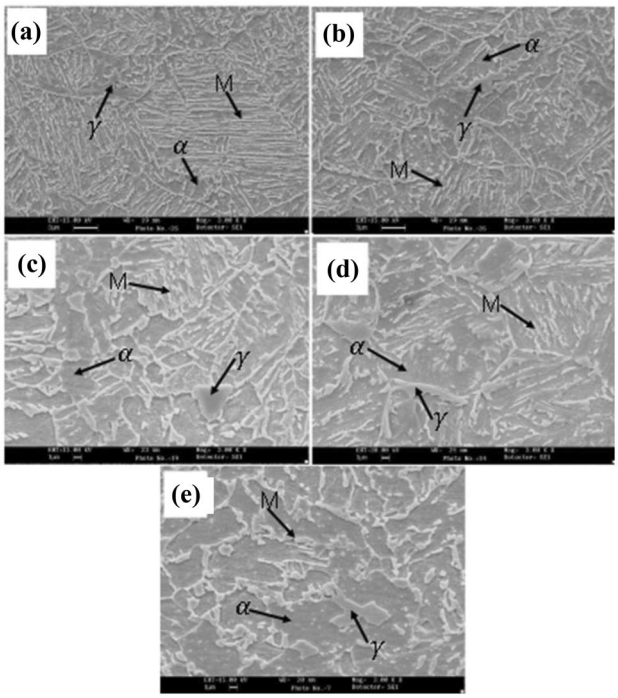

Fig. 11 SEM images of the samples partitioned at 390 °C for 10 (**a**), 100 (**b**), 300 (**c**), 500 (**d**) and 1000 s (**e**)

dominant phase in the final microstructure of these samples was M. V_{γ_R} was continually increased by increasing Pt up to 500 s (Fig. 13). The XRD patterns for the samples partitioned at 390 °C for 10–1000 s are shown in Fig. 12a–e. The structural characteristics for these samples calculated from the XRD data are summarized in Table 4. The highest V_{γ_R}% of ~ 36.1% was obtained for the sample partitioned at 390 °C for 500s. V_{γ}% in the sample partitioned 390 °C

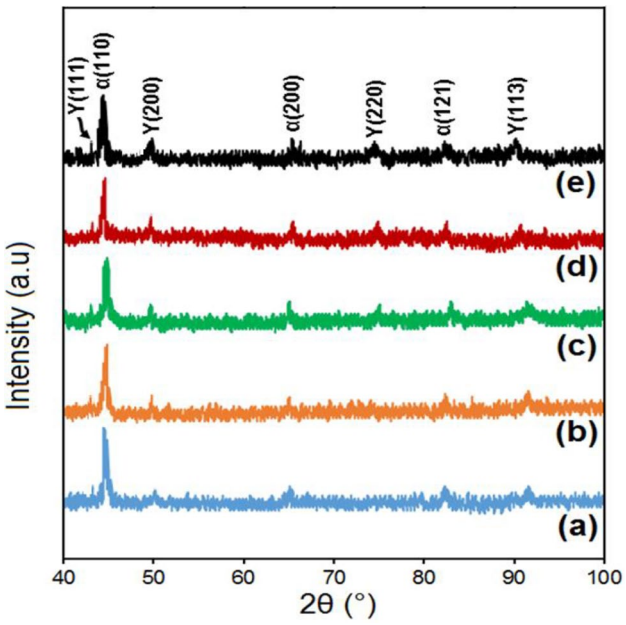

Fig. 12 XRD patterns of the samples partitioned at the temperature of 390 °C for 10 (**a**), 100 (**b**), 300 (**c**), 500 (**d**) and 1000 s (**e**)

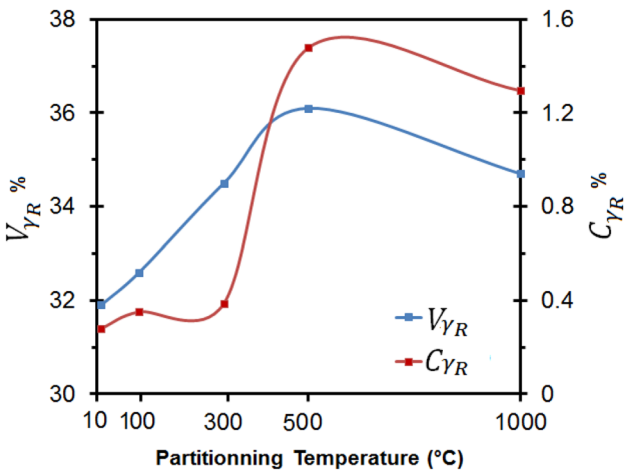

Fig. 13 Variations in V_{γ_R} and C_{γ_R} as a function of Pt

Table 4 Structural characteristics of the samples partitioned at 390 °C for 10–1000 s

Sample name	V_{γ_R}, %	$\theta_{(200)\gamma}$, °	a_γ, °A	C_{γ_R}, wt.%
Pt-10 s	31.9	25.66	3.560	0.28
Pt-100 s	32.6	25.609	3.563	0.35
Pt-300 s	34.5	25.594	3.564	0.39
Pt-500 s	36.1	25.213	3.615	1.48
Pt-1000 s	34.7	25.291	3.606	1.29

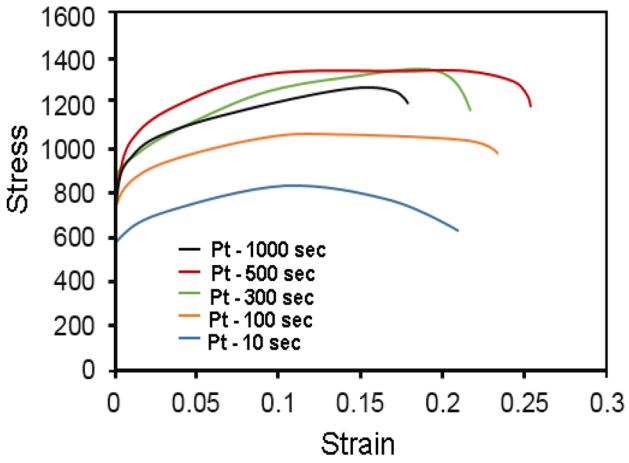

Fig. 14 Stress–strain curves for the samples partitioned at 390 °C for 10–1000 s

Table 5 Mechanical properties of the samples partitioned at 390 °C for 10–1000 s

Sample designation	UTS, MPa	Y.S, MPa	Total elongation, %
Pt-10 s	846 ± 4	556 ± 4	21.32 ± 0.5
Pt-100 s	1075 ± 9	733 ± 7	23.82 ± 0.9
Pt-300 s	1353 ± 5	742 ± 5	21.96 ± 0.4
Pt-500 s	1366 ± 3	741 ± 9	25.18 ± 0.6
Pt-1000 s	1256 ± 7	761 ± 3	17.75 ± 0.9

for 1000 s was lower ($V_\gamma = 34.7\%$) than that of the sample partitioned for 500 s ($V_\gamma = 36.1\%$). This could be due to the more increasing the grain size of ferrite by extending the Pt to 1000 s.

The tensile stress–strain curves for the samples partitioned at 390 °C for 10–1000 s are illustrated in Fig. 14. UTS, YS, and total elongation for these samples are given in Table 5. The YS of the samples was increased by increasing Pt up to 1000 s, however, the UTS increased by increasing the Pt up to 500 s and then decreased by further increasing the Pt to 1000 s due to supersaturated of V_{γ_R} by carbon. The area under the stress–strain curves in the samples partitioned at 390 °C for 300–500 s is larger than those of the other samples (Fig. 14). Thus, it could be concluded that the toughness (ductility) of the samples partitioned at 390 °C in the time interval 300–500 s is higher than that of the others. The results show that the tensile strength of the sample partitioned for 1000 s is smaller than that of the sample partitioned for 500 s. The lower V_{γ_R} of the former has resulted in the lower strength. This feature led to production of the lower martensite produced from strain-induced austenite, which resulted in the lower strength of Pt-1000 s compare to the sample of Pt-500 s. As seen in Fig. 15, maximum hardness was recorded for the sample partitioned at 390 °C for 500 s (~ 322 HB)

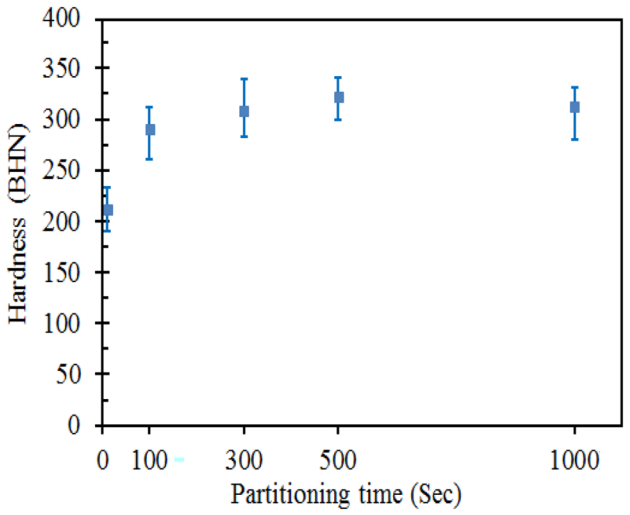

Fig. 15 Hardness of the samples partitioned at 390 °C for 10–1000 s

due to the higher C_{γ_R} of γ_R. Summarizing the results, it could be concluded that at PT of ~ 390 °C, a Pt of 500 s is the best for Q–P process for the steel investigated in the present research.

Conclusions

The V_{γ_R} in the Q–P process is effectively controlled by PT and Pt, i.e., by increasing the PT or Pt in their suitable range, V_{γ_R} is increased. V_{γ_R} in the partitioned samples was increased from 7.68 to 28.10% by increasing the PT from 290 to 390 °C and then decreased to 22.51% by further increasing the PT to 410 °C. According to the results obtained within the scope of the present study, the temperature interval of 370–410 °C was recognized as the suitable PT because of higher V_{γ_R}, higher UTS, higher hardness and lower Y.S. Also, the effects of Pt (10, 100, 300, 500 and 1000 s) at the PT of 390 °C were evaluated. Increasing Pt from 10 to 500 s at PT of 390 °C resulted in an increase in V_{γ_R} from 31.9 to 36.1%. The V_{γ_R} in the sample partitioned at 390 °C for 1000 s showed some reduction in comparison to that of the sample partitioned at that temperature for ~ 500 s. However, the UTS, hardness and total elongation of the samples increased up to the Pt of 500 s and then decreased in the sample partitioned for 1000 s. Considering the UTS, YS, total elongation, toughness and BHN, within the samples investigated in the present study, it is concluded that a PT of 390 °C and a Pt of 500 s could be the best partitioning temperature and time for the Q–P process in the present steel.

References

1. R.D.K. Misra, H. Nathani, J.E. Hartmann, F. Siciliano, Microstructural evolution in a new 770 MPa hot rolled Nb–Ti microalloyed steel. Mater. Sci. Eng. A **394**, 339–352 (2005). https://doi.org/10.1016/j.msea.2004.11.041
2. P. Liu, X. Yu, K. Wang, B. Zhu, J. Li, Y. Zhang, A new hot stamping process with quenching and partitioning treatment. Adv. Mater. Res. **1095**, 673–676 (2015). https://doi.org/10.4028/www.scientific.net/AMR.1095.673
3. J. Dong, C. Li, C. Liu, Y. Huang, L. Yu, H. Li, Y. Liu, Microstructural and mechanical properties development during quenching-partitioning-tempering process of Nb-V-Ti micro alloyed ultra-high strength steel. Mater. Sci. Eng. A **705**, 249–256 (2017). https://doi.org/10.1016/j.msea.2017.08.081
4. K. Zhang, P. Liu, W. Li, F. Ma, Z. Guo, Y. Rong, Enhancement of the strength and ductility of martensitic steels by carbon. Mater. Sci. Eng. A **716**, 87–91 (2018). https://doi.org/10.1016/j.msea.2018.01.012
5. A.J. Clarke, J.G. Speer, M.K. Miller, R.E. Hackenberg, D.V. Edmonds, D.K. Matlock, F.C. Rizzo, K.D. Clarke, E. De Moor, Carbon partitioning to austenite from martensite or bainite during the quench and partition (Q&P) process: a critical assessment. Acta Mater. **56**, 16–22 (2008). https://doi.org/10.1016/j.actamat.2007.08.051
6. J. Park, M.C. Jo, T. Song, H.S. Kim, S.S. Sohn, S. Lee, Ultra-high strength and excellent ductility in multi-layer steel sheet of austenitic hadfield and martensitic hot-press-forming steels. Mater. Sci. Eng. A **759**, 320–328 (2019). https://doi.org/10.1016/j.msea.2019.05.046
7. R. Blonde, E.J. Melero, L. Zhao, J.P. Wright, E. Brück, S. Van Der Zwaag, N.H. Van Dijk, High-energy X-ray diffraction study on the temperature-dependent mechanical stability of retained austenite in low-alloyed TRIP steels. Acta Mater. **60**, 565–577 (2012). https://doi.org/10.1016/j.actamat.2011.10.019
8. G. Bansal, M. Pradeep, C. Ghosh, V. Rajinikanth, V.C. Srivastava, V.A. Bhagat, S. Kundu, Evolution of microstructure in a low-Si micro-alloyed steel processed through one-step quenching and partitioning. Metall. Mater. Trans. A **50**, 547–555 (2019). https://doi.org/10.1007/s11661-018-5039-8
9. J. Hang, H. Ding, R. Misra, C. Wang, Microstructural evolution and consequent strengthening through niobium-microalloying in a low carbon quenched and partitioned steel. Mater. Sci. Eng. A **641**, 242–248 (2015). https://doi.org/10.1016/j.msea.2015.06.050
10. E.P. Uorinen, A.G. Özügürler, J.C. Ion, K. Eriksson, M.C. Somani, L.P. Karjalainen, S. Allain, F.G. Caballero, Hot forming of ultra-fine-grained multiphase steel products using press hardening combined with quenching and partitioning process. Metals **9**, 357 (2019). https://doi.org/10.3390/met9030357
11. P. Huyghe, L. Malet, M. Caruso, C. Georges, S. Godet, On the relationship between the multiphase microstructure and the mechanical properties of a 0.2 C quenched and partitioned steel. Mater. Sci. Eng. A **701**, 254–263 (2017). https://doi.org/10.1016/j.msea.2017.06.058
12. D. De Knijf, C. Föjer, L.A.I. Kestens, R. Petrov, Factors influencing the austenite stability during tensile testing of Quenching and Partitioning steel determined via in situ electron backscatter diffraction. Mater. Sci. Eng. A **638**, 219–227 (2015). https://doi.org/10.1016/j.msea.2015.04.075
13. D. De Knijf, E.P. Da Silva, C. Föjer, R. Petrov, Study of heat treatment parameters and kinetics of quenching and partitioning cycles. Mater. Sci. Technol. **31**, 817–828 (2015). https://doi.org/10.1179/1743284714Y.0000000710
14. D. De Knijf, R. Petrov, C. Föjer, L.A.I. Kestens, Effect of fresh martensite on the stability of retained austenite in quenching and

partitioning steel. Mater. Sci. Eng. A **615**, 107–115 (2014). https://doi.org/10.1016/j.msea.2014.07.054
15. G. Khalaj, H. Pouraliakbar, K.R. Mamaghani, M.J. Khalaj, Modeling the correlation between heat treatment, chemical composition and bainite fraction of pipeline steels by means of artificial neural networks. Neural Netw. World **1**, 351–368 (2013)
16. J. Zhang, H. Ding, R. Misra, C. Wang, Microstructural evolution and consequent strengthening through niobium-microalloying in a low carbon quenched and partitioned steel. Mater. Sci. Eng. A **641**, 242–248 (2015). https://doi.org/10.1016/j.msea.2015.06.050
17. L.L. Wu, T.K. Yao, J.W. Zhang, F.R. Xiao, Understanding the mechanical properties of vanadium carbides: nano-indentation measurement and first-principles calculations. J. Alloys Compd. **548**, 60–64 (2013). https://doi.org/10.1016/j.jallcom.2012.09.014
18. Z. Xiaosheng, L. Chenxi, Y. Liming, L. Yongchang, L. Huijun, Phase transformation behavior and microstructural control of high-Cr martensitic/ferritic heat-resistant steels for power and nuclear plants: a review. J. Mater. Sci. Technol. **31**, 235–242 (2015). https://doi.org/10.1016/j.jmst.2014.12.001
19. D.T. Pierce, D.R. Coughlin, D.L. Williamson, K.D. Clarke, A.J. Clarke, J.G. Speer, E. De Moor, Characterization of transition carbides in quench and partitioned steel microstructures by Mössbauer spectroscopy and complementary techniques. Acta Mater. **90**, 417–430 (2015). https://doi.org/10.1016/j.actamat.2015.01.024
20. S. Yan, X. Liu, Microstructure and mechanical properties of a low-carbon steel treated by one-step quenching and partitioning process. Adv. Mater. Res. **1082**, 202–207 (2015). https://doi.org/10.4028/www.scientific.net/AMR.1082.202
21. N. Zhong, Q. Wu, Y. Yin, X. Wang, Micro-structural evolution of a medium carbon advanced high strength steel heat-treated by quenching-partitioning process. Steel Res. Int. **86**, 252–256 (2015). https://doi.org/10.1002/srin.201400064
22. Y. Toji, G. Miyamoto, D. Raabe, Carbon partitioning during quenching and partitioning heat treatment accompanied by carbide precipitation. Acta Mater. **86**, 137–147 (2015). https://doi.org/10.1016/j.actamat.2014.11.049
23. P. Liu, B. Zhu, Y. Wang, Y. Zhang, Coupled model for carbon partitioning from martensite into austenite during the quenching process in Fe–C steels. Miner. Met. Mater. Soc. ASM Int. (2016). https://doi.org/10.1007/s11661-016-3560-1
24. F. Peng, Y. Xu, J. Li, X. Gu, X. Wang, Interaction of martensite and bainite transformations and its dependence on quenching temperature in intercritical quenching and partitioning steel. Mater. Des. **181**, 107921 (2019). https://doi.org/10.1016/j.matdes.2019.107921
25. M.J. Santofimia, J.G. Speer, A.J. Clarke, L. Zhao, J. Sietsma, Influence of interface mobility on the evolution of austenite–martensite grain assemblies during annealing. Acta Mater. **57**(15), 4548–4557 (2009). https://doi.org/10.1016/j.actamat.2009.06.024
26. V.F. Zackay, M.D. Bhandarkar, E.R. Parker, The role of deformation-induced phase transformations in the plasticity of some iron-based alloys, in *Advances in Deformation Processing* (1978), pp. 351–404
27. P. Kantanen, M. Somani, A. Kaijalainen, O. Haiko, D. Porter, J. Komi, Microstructural characterization and mechanical properties of direct quenched and partitioned high-aluminum and high-silicon steels. Metals **9**, 256 (2019). https://doi.org/10.3390/met9020256
28. M. Pozuelo, J.W. Stremfel, J.M. Yang, J. Marian, Strengthening to softening transition in lath martensite. Materialia **5**, 100254 (2019). https://doi.org/10.1016/j.mtla.2019.100254
29. M. Cheng, H.W. Song, X. Li, S.H. Zhang, T. Lin, Effects of quenching and partitioning process on mechanical properties of a hot-stamping steel. Mater. Sci. Forum **788**, 340–345 (2014). https://doi.org/10.1007/s42243-018-0183-3
30. S. Kim, C.G.I.L. Lee, I. Choi, S. Lee, Effects of heat treatment and alloying elements on the microstructures and mechanical properties of 0.15 wt. Pct C transformation-induced plasticity-aided cold-rolled steel sheets. Metall. Mater. Trans. A **32**, 505–514 (2001). https://doi.org/10.1007/s11661-001-0067-0
31. E.C. Bain, *Functions of Alloying Elements in Steel*, 1st edn (ASM International, Chicago, 1939)
32. H. Bhadeshia, R. Honeycombe, *Steels: Microstructure and Properties*, 3rd edn (Elsevier Inc., Amsterdam, 2006)
33. J. Tobata, K.L. Ngo-Huynh, N. Nakada, T. Tsuchiyama, S. Takaki, Role of silicon in quenching and partitioning treatment of low-carbon martensitic stainless steel. ISIJ Int. **52**, 1377–1382 (2012). https://doi.org/10.2355/isijinternational.52.1377
34. J. Mahieu, B.C. Cooman, S. Claessens, Galvanizability of high-strength steels for automotive applications. Metall. Mater. Trans. A **32**, 2905–2908 (2001). https://doi.org/10.1007/s11661-001-1042-5
35. M. De Meyer, D. Vanderschueren, B.C. De Cooman, K.E.Y. Wor, The influence of the substitution of Si by Al on the properties of cold rolled C-Mn-Si TRIP steels. ISIJ Int. **39**, 813–822 (1999). https://doi.org/10.2355/isijinternational.39.813
36. E.S. Rowland, S.R. Lyle, The application of MS points to case depth measurement. Trans. ASM **37**, 27–47 (1946)
37. S. Hartmann, H. Ruppersberg, Thermal expansion of cementite and thermo-elastic stresses in white cast iron. Mater. Sci. Eng. A **190**, 231–239 (1995). https://doi.org/10.1016/0921-5093(94)09616-5
38. C.F. Jatczak, *Retained Austenite and Its Measurement By X-Ray Diffraction* (SAE International, Warrendale, 1980)